J|A|C|S
ARTICLES
Published on Web 07/14/2005

Diferrous Cyanides as Models for the Fe-only Hydrogenases

Christine A. Boyke,[†] Jarl Ivar van der Vlugt,[†] Thomas B. Rauchfuss,*[,†]
Scott R. Wilson,[†] Giuseppe Zampella,[‡] and Luca De Gioia*[,‡]

Contribution from the Department of Chemistry, University of Illinois at Urbana-Champaign, Urbana, Illinois 61801, and Department of Biotechnology and Biosciences, University of Milano-Bicocca, Piazza della Scienza 1 20126-Milan

Received March 11, 2005; E-mail: rauchfuz@uiuc.edu

Abstract: The first systematic study of diferrous dicyano dithiolates is described. Oxidation of $[Fe_2(S_2C_2H_4)(CN)_2(CO)_4]^{2-}$ in the presence of cyanide and tertiary phosphines and of $Fe_2(S_2C_2H_4)(CO)_4(PMe_3)_2$ in the presence of cyanide affords a series of diferrous cyanide derivatives that bear a stoichiometric, structural, and electronic relationship to the H_{ox}^{air} state of the Fe-only hydrogenases. With PPh_3 as the trapping ligand, we obtained an unsymmetrical isomer of $Fe_2(S_2C_2H_4)(\mu\text{-CO})(CN)_2(PPh_3)_2(CO)_2$, as confirmed crystallographically. This diferrous cyanide features the *semi*bridging CO-ligand, with Fe-μC bond lengths of 2.15 and 1.85 Å. Four isomers of $Fe_2(S_2C_2H_4)(\mu\text{-CO})(CN)_2(PMe_3)_2(CO)_2$ were observed, the initial product again being unsymmetrical but more stable isomers being symmetrical. DFT calculations confirm that the most stable isomers of $Fe_2(S_2C_2H_4)(\mu\text{-CO})(CN)_2(PMe_3)_2(CO)_2$ have cyanide trans to μ-CO. Oxidative decarbonylation also afforded the new tetracyanide $[Fe_2(S_2C_2H_4)(\mu\text{-CO})(CN)_4(CO)_2]^{2-}$. Insights into the oxidative decarbonylation mechanism of these syntheses come from the spectroscopic characterization of the tetracarbonyl $[Fe_2(S_2C_2H_4)(\mu\text{-CO})(CN)_3(CO)_3]^-$. This species reacts with PEt_3 to produce the stable adduct $[Fe_2(S_2C_2H_4)(\mu\text{-CO})(CN)_3(CO)_2(PEt_3)]^-$.

Introduction

The Fe-only hydrogenases are highly efficient catalysts for hydrogen evolution and oxidation. The unusual structure of the active site of these enzymes, together with the technological implications of their reactivity, has attracted intense interest from both biological and chemical scientists.[1,2] The H-cluster active site contains CO and CN^- ligands as well as a novel dithiolate cofactor, as deduced from a combination of crystallographic analysis[3] and spectroscopic data.[4] Four principal states of the active site are known (Figure 1), with H_{ox} and H_{red} as being catalytically active. The collective evidence points to the oxidation state assignments $[Fe^{II}Fe^{I}]$ ($S = {}^1/_2$) for H_{ox} and $[Fe^{II}Fe^{II}]$ for H_{red}, respectively, the latter being a protonated $[Fe^{I}Fe^{I}]$ species, hence the formal Fe(II) assignment.[5]

Inhibition of H_{ox} (and H_{red}) by CO yields H_{ox}^{CO},[6−8] which is also an $S = {}^1/_2$ species. The exogenous CO occupies the coordination site proposed to be directly involved in dihydrogen activation and production.[9] Air deactivation converts the bimetallic subunit of the H cluster to the diamagnetic H_{ox}^{air} state, which is proposed to be $[Fe^{II}Fe^{II}]$.

Initial modeling studies focused on substituted modifications of $Fe_2(SR)_2(CO)_6$ and their protonated derivatives.[10,11] Our early studies identified $[Fe_2(S_2C_3H_6)(CN)_2(CO)_4]^{2-}$ as a first generation structural model for the active site,[12] while biomimetic catalysis was discovered with $HFe_2(S_2C_3H_6)(CN)(PMe_3)(CO)_4$.[13] Subsequent work has confirmed the general applicability of diiron dithiolates for catalytic production of H_2 by proton reduction.[14−17]

A major challenge is the synthesis of active site models that more faithfully replicate the structural features of the natural system, as identified crystallographically.[18] To this end, we recently described a new class of diiron dithiolates of the formula $[Fe_2(S_2C_nH_{2n})(\mu\text{-CO})(CNMe)_6]^{2+}$ obtained from oxida-

[†] University of Illinois at Urbana-Champaign.
[‡] University of Milano-Bicocca.

(1) Frey, M. *ChemBioChem* **2002**, *3*, 153−160.
(2) Cammack, R.; Frey, M.; Robson, R. *Hydrogen as a Fuel: Learning from Nature*; Taylor & Francis: London, 2001.
(3) Nicolet, Y.; Lemon, B. J.; Fontecilla-Camps, J. C.; Peters, J. W. *Trends Biochem. Sci.* **2000**, *25*, 138−143.
(4) Pierik, A. J.; Hulstein, M.; Hagen, W. R.; Albracht, S. P. J. *Eur. J. Biochem.* **1998**, *258*, 572−578.
(5) Liu, Z.-P.; Hu, P. *J. Am. Chem. Soc.* **2002**, *124*, 5175−5182.
(6) Lemon, B. J.; Peters, J. W. *Biochemistry* **1999**, *38*, 12969−12973.
(7) Lemon, B. J.; Peters, J. W. *J. Am. Chem. Soc.* **2000**, *122*, 3793−3794.
(8) Chen, Z.; Lemon, B. J.; Huang, S.; Swartz, D. J.; Peters, J. W.; Bagley, K. A. *Biochemistry* **2002**, *41*, 2036−2043.
(9) De Lacey, A. L.; Stadler, C.; Cavazza, C.; Hatchikian, E. C.; Fernandez, V. M. *J. Am. Chem. Soc.* **2000**, *122*, 11232−11233.
(10) Evans, D. J.; Pickett, C. J. *Chem. Soc. Rev.* **2003**, *32*, 268−275.
(11) Georgakaki, I. P., Darensbourg, M. Y. In *Comprehensive Coordination Chemistry II*; McCleverty, J. A., Meyer, T. J., Eds.: Amsterdam, 2004.
(12) Schmidt, M.; Contakes, S. M.; Rauchfuss, T. B. *J. Am. Chem. Soc.* **1999**, *121*, 9736−9737.
(13) Gloaguen, F.; Lawrence, J. D.; Rauchfuss, T. B.; Bénard, M.; Rohmer, M.-M. *Inorg. Chem.* **2002**, *41*, 6573−6582.
(14) Borg, S. J.; Behrsing, T.; Best, S. P.; Razavet, M.; Liu, X.; Pickett, C. J. *J. Am. Chem. Soc.* **2004**, *126*, 16988−16999.
(15) Cheah, M. H.; Borg, S. J.; Bondin, M. I.; Best, S. P. *Inorg. Chem.* **2004**, *43*, 5635−5644.
(16) Mejia-Rodriguez, R.; Chong, D.; Reibenspies, J. H.; Soriaga, M. P.; Darensbourg, M. Y. *J. Am. Chem. Soc.* **2004**, *126*, 12004−12014.
(17) Chong, D.; Georgakaki, I. P.; Mejia-Rodriguez, R.; Sanabria-Chinchilla, J.; Soriaga, M. P.; Darensbourg, M. Y. *Dalton Trans.* **2003**, 4158−4163.
(18) Tard, C.; Liu, X.; Ibrahim, S. K.; Bruschi, M.; De Gioia, L.; Davies, S. C.; Yang, X.; Wang, L.-S.; Sawers, G.; Pickett, C. J. *Nature* **2005**, *433*, 610−614.

10.1021/ja051584d CCC: $30.25

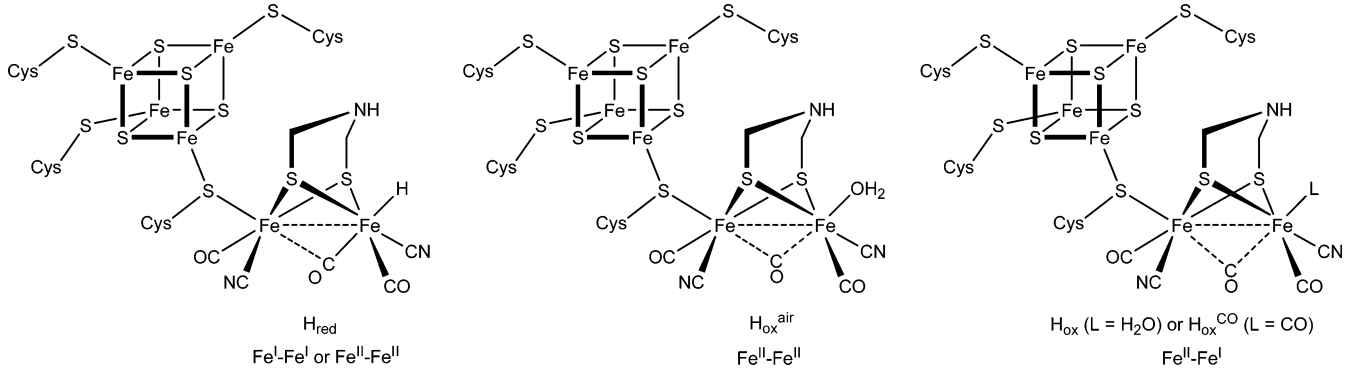

Figure 1. Structures of the four states of the active sites of Fe-only hydrogenases.

tive decarbonylation of the classical[19−21] substituted derivatives of $Fe_2(SR)_2(CO)_4L_2$ species. The resulting complexes replicate key features of H_{ox}^{air}: a face-sharing bioctahedral structure, diamagnetism, a short Fe−Fe distance, and a μ-CO ligand.[22] Several structural aspects of the coordination environment remain to be modeled, including the incorporation of naturally occurring ligands on the diferrous framework, in particular CN^- and CO ligands, as observed in all forms of the binuclear active site.

Diferrous cyanides were first detected by Pickett et al. in studies on the electrochemical oxidation of $[Fe_2[(SCH_2)_2CHCH_2SMe](CN)_2(CO)_4]^{2-}$, a di-subferrous species containing a pendant thioether.[23] Low-temperature oxidation of this species afforded an unstable intermediate with FT-IR and EPR signatures characteristic of a mixed valence derivative. This H_{ox}^{CO} model undergoes further $1e^-$ oxidation to give an unstable diferrous derivative. Diferrous cyanides formally arise from the protonation of $[Fe_2(S_2C_3H_6)(CN)_2(CO)_4]^{2-}$ and $[Fe_2(S_2C_3H_6)(CN)(CO)_4(PMe_3)]^-$,[13,24] although these species contain μ-H ligands. Liaw and co-workers have described routes to both monoferrous cyanides[25] including $[Fe(SR)_2(CN)(CO)_2L]^-$ (L = CO, SR_2), $[Fe(SR)(CN)_3(CO)_2]^{2-}$, and diferrous tetracyanides $[Fe_2(\mu\text{-SEt})_2(CN)_4(CO)_4]^{2-}$.[26]

An obvious approach to diferrous dithiolato dicyanides is the oxidation of $[Fe_2(SR)_2(CN)_2(CO)_4]^{2-}$, but our early attempts afforded only insoluble mixtures.[12] In this paper we revisit this synthetic challenge, capitalizing on our recently discovered route to $[Fe_2(SR)_2(\mu\text{-CO})(CNMe)_6]^{2+}$ which entailed the use of milder oxidation conditions in the presence of soft trapping ligands (eq 1).[22]

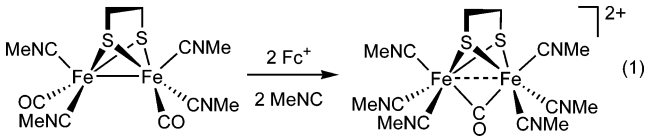

Results and Discussion

Synthesis of Diferrous Dicyanides. The basic method entails oxidation of MeCN solutions of $(Et_4N)_2[Fe_2(S_2C_2H_4)(CN)_2(CO)_4]$, $(Et_4N)_2$(**1**), with 2 equiv of $FcPF_6$ in the presence of tertiary phosphines. The reactions proceed more efficiently when conducted under an atmosphere of CO at −40 °C. The complex ^{31}P NMR spectra of the crude red reaction mixtures indicate the presence of several products. Purification by recrystallization and column chromatography proved useful for obtaining three species in pure form (Scheme 1).

A. $Fe_2(S_2C_2H_4)(\mu\text{-CO})(CN)_2(PPh_3)_2(CO)_2$ (2). Oxidation of $(Et_4N)_2$(**1**) in the presence of excess PPh_3 (Scheme 1) gave stable homogeneous solutions. Despite the simplicity of the IR spectrum, the complex ^{31}P NMR spectrum indicated that the reaction mixture contained several isomers. Using a combination of column chromatography and fractional crystallization, we were able to isolate one isomer of $Fe_2(S_2C_2H_4)(\mu\text{-CO})(CN)_2(PPh_3)_2(CO)_2$ (**2**) in 10% yield. ^{31}P NMR analysis of the crude reaction mixture indicates that **2** is the major product of the reaction, formed in ca. 25% yield. ^{31}P NMR spectroscopy revealed that the two phosphine ligands in **2** are chemically nonequivalent. The FT-IR spectrum of **2** exhibited weak bands at 2119 and 2104 cm^{-1} assigned to ν_{CN}, strong bands at 2040 and 1993 cm^{-1} assigned to ν_{CO}, and a broader band of medium intensity at 1904 cm^{-1} attributed to $\nu_{\mu-CO}$.

The crystallographically determined structure for **2** confirms its face-sharing bioctahedral core (Figure 2, Table 1).[22,27] The bridging CO ligand is coordinated asymmetrically, reflecting the electronically disparate trans ligands, PPh_3 and CN^-, with bond lengths of 2.15 Å for Fe(1)−C(39) and 1.85 Å for Fe(2)−C(39). The shorter Fe(2)−C(μ) distance is attributed to the influence of the strongly σ-donating trans cyanide. The *semi*-bridging character[28] of the μ-CO-ligand is further indicated by the Fe−C(μ)−O angles 129.8° and 151.4°. The Fe(1)−Fe(2) distance is 2.55 Å, which is close to the values found in the enzymes CpI and DdH,[3] but this parameter is rather insensitive for a wide range of bioctahedral diiron species. We have previously discussed the fact that species of the type $Fe^{I}_2(SR)_2L_6$ contain an Fe−Fe bond,[29] whereas the related $Fe^{II}_2(SR)_2(\mu\text{-CO})L_6$ species feature 3-center-2-electron interactions involving the bridging CO ligand.[22,30] The different steric properties of the axial CN^- and PPh_3 are reflected in the geometry around the respective iron centers; i.e., the S(1)−Fe(1)−P(1) angle is 99.62°, while the related S(1)−Fe(2)−C(43)N angle is 90°.

(19) de Beer, J. A.; Haines, R. J. *J. Organomet. Chem.* **1972**, *36*, 297−313.
(20) de Beer, J. A.; Haines, R. J. *J. Organomet. Chem.* **1972**, *37*, 173−188.
(21) Fauvel, K.; Mathieu, R.; Poilblanc, R. *Inorg. Chem.* **1976**, *15*, 976−978.
(22) Boyke, C. A.; Rauchfuss, T. B.; Wilson, S. R.; Rohmer, M.-M.; Bénard, M. *J. Am. Chem. Soc.* **2004**, *126*, 15151−15160.
(23) Razavet, M.; Davies, S. C.; Hughes, D. L.; Barclay, J. E.; Evans, D. J.; Fairhurst, S. A.; Liu, X.; Pickett, C. J. *Dalton Trans.* **2003**, 586−595.
(24) Zhao, X.; Georgakaki, I. P.; Miller, M. L.; Yarbrough, J. C.; Darensbourg, M. Y. *J. Am. Chem. Soc.* **2001**, *123*, 9710−9711.
(25) Chen, C.-H.; Chang, Y.-S.; Yang, C.-Y.; Chen, T.-N.; Lee, C.-M.; Liaw, W.-F. *Dalton Trans.* **2004**, 137−143.
(26) Liaw, W.-F.; Tsai, W.-T.; Gau, H.-B.; Lee, C.-M.; Chou, S.-Y.; Chen, W.-Y.; Lee, G.-H. *Inorg. Chem.* **2003**, *42*, 2783−2788.
(27) Lawrence, J. D.; Rauchfuss, T. B.; Wilson, S. R. *Inorg. Chem.* **2002**, *41*, 6193−6195.
(28) Cotton, F. A.; Kruczynski, L.; Frenz, B. A. *J. Organomet. Chem.* **1978**, *160*, 93−100.

Scheme 1

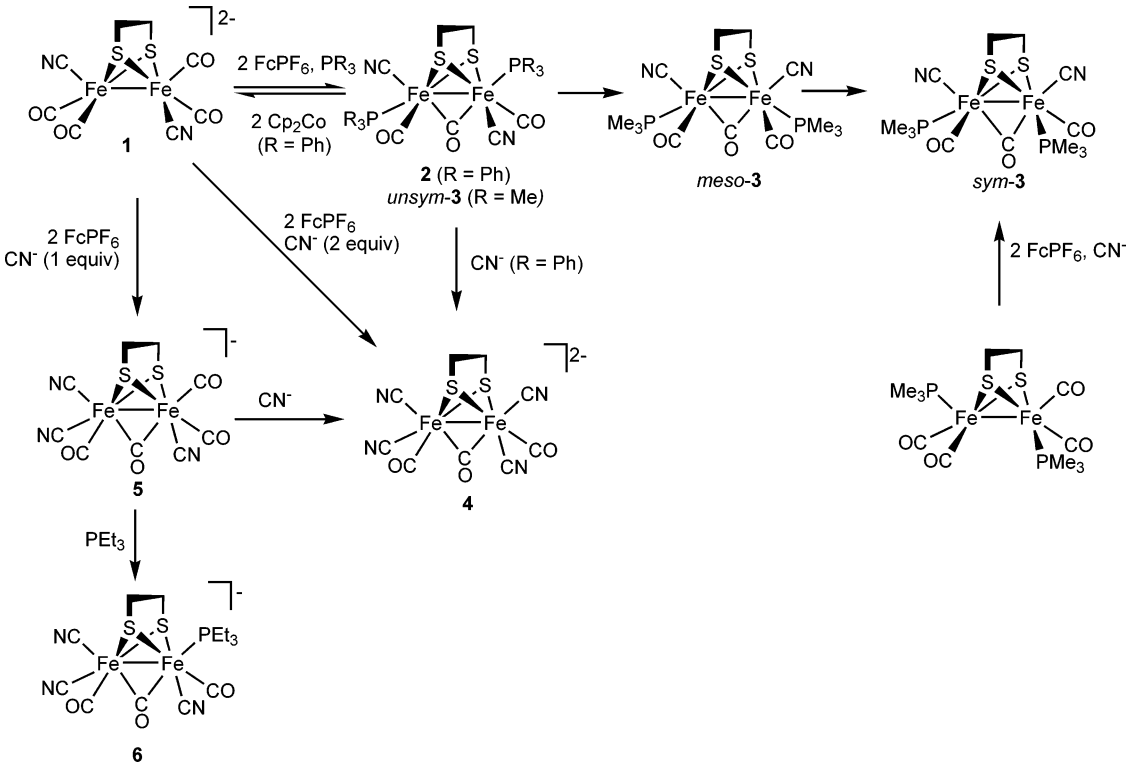

Table 1. Selected Bond Lengths (Å) and Angles (deg) for $Fe_2(S_2C_2H_4)(\mu\text{-CO})(CN)_2(PPh_3)_2(CO)_2$, **2**

Fe(1)−S(1)	2.239(2)	Fe(1)−S(2)	2.256(2)
Fe(2)−S(1)	2.268(2)	Fe(2)−S(2)	2.278(2)
Fe(1)−C(39)	2.148(7)	Fe(2)−C(39)	1.853(7)
Fe(1)−P(1)	2.260(2)	Fe(2)−C(43)	1.938(7)
Fe−Fe	2.5461(17)	S(1)−Fe(1)−P(1)	99.62(8)
S(1)−Fe(2)−C(43)	88.9(2)	Fe(1)−C(39)−Fe(2)	78.7(3)
P(1)−Fe(1)−C(39)	162.33(19)	C(43)−Fe(2)−C(39)	168.3(3)
Fe(1)−C(39)−O(1)	129.8(6)	Fe(2)−C(39)−O(1)	151.4(6)
C(39)−Fe(1)−Fe(2)	45.52(18)	C(39)−Fe(2)−Fe(1)	55.8(2)

B. $Fe_2(S_2C_2H_4)(\mu\text{-CO})(CN)_2(PMe_3)_2(CO)_2$ (3). As in the PPh_3 case, oxidation of $(Et_4N)_2$(**1**) in the presence of PMe_3 (Scheme 1) also gave a homogeneous mixture, as indicated by ^{31}P NMR and IR analysis. Workup by column chromatography afforded $Fe_2(S_2C_2H_4)(\mu\text{-CO})(CN)_2(PMe_3)_2(CO)_2$ (*unsym*-**3**), which is structurally analogous to **2**. The FT-IR (Figure 3) and ^{31}P NMR spectra are unexceptional, although the two phosphine signals were observed as doublets in the ^{31}P NMR spectrum, with a coupling constant $^3J_{P-P}$ of 6 Hz. The IR band for the μ-CO-ligand is present at 1884 cm^{-1}, 20 cm^{-1} lower in energy vs **2**.

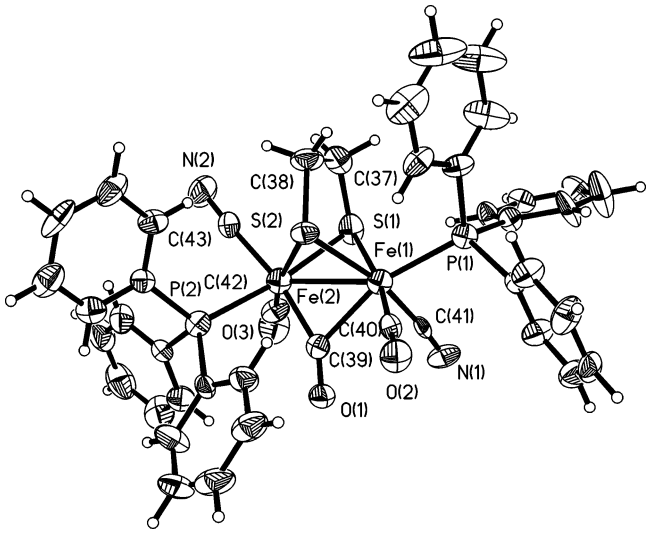

Figure 2. Structure of $Fe_2(S_2C_2H_4)(\mu\text{-CO})(CN)_2(PPh_3)_2(CO)_2$, **2**. Thermal ellipsoids are drawn at the 50% probability level.

We examined a complementary route to **3** via oxidative decarbonylation of the bisphosphine $Fe_2(S_2C_2H_4)(CO)_4(PMe_3)_2$[13] using cyanide as the trapping ligand (Scheme 1). This reaction yielded a red-brown homogeneous solution, for which the ^{31}P NMR spectrum, however, did *not* indicate the presence of *unsym*-**3**. Instead, an extractive workup using toluene afforded a symmetrical isomer of $Fe_2(S_2C_2H_4)(\mu\text{-CO})(CN)_2(PMe_3)_2(CO)_2$, *sym*-**3**. In contrast to *unsym*-**3**, the ^{31}P NMR spectrum of *sym*-**3** consisted of a singlet for the two equivalent PMe_3 ligands. The FT-IR spectrum revealed a single medium ν_{CN} band at 2115 cm^{-1}, as well as bands at 2020 (shoulder), 2003, and 1839 cm^{-1} (ν_{CO}), indicative of a C_2 isomer (Figure 3). We were unable to grow crystals of *sym*-**3**, but its structure was analyzed by DFT calculations (vide infra).

Using ^{31}P NMR and FT-IR spectroscopy, we observed traces of *sym*-**3** in samples of *unsym*-**3**. In situ NMR spectroscopic measurements confirmed that *unsym*-**3** indeed converts to *sym*-**3** (Figure 4), i.e., that *unsym*-**3** is a kinetic isomer formed from oxidative decarbonylation of $(Et_4N)_2$(**1**). Interestingly, our in situ experiments revealed two intermediates in the conversion of *unsym*-**3** into *sym*-**3**. The first intermediate is symmetrical (one ^{31}P NMR resonance), which we suggest is the meso isomer, *meso*-**3** (Figure 4). Concomitant with the disappearance of

(29) Dahl, L. F.; Wei, C. H. *Inorg. Chem.* **1963**, *2*, 328−333.
(30) Lawrence, J. D.; Rauchfuss, T. B.; Wilson, S. R. *Inorg. Chem.* **2002**, *41*, 6193−6195.

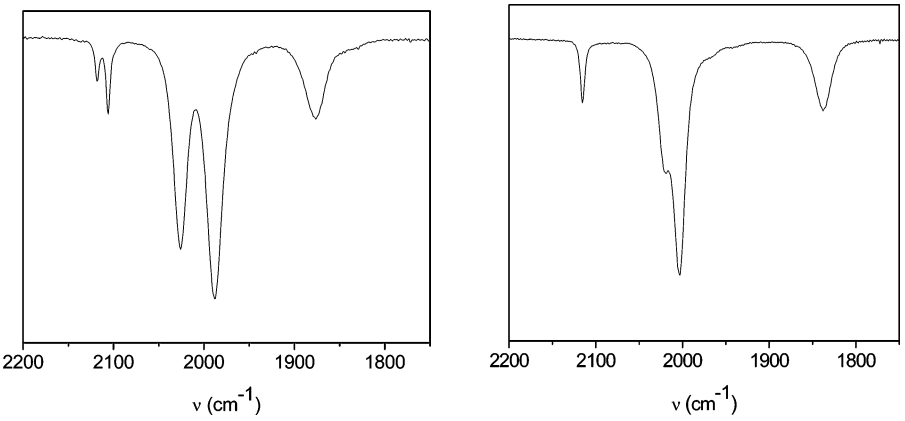

Figure 3. FT-IR spectra (MeCN) of *unsym*-**3** (left) and *sym*-**3** (right).

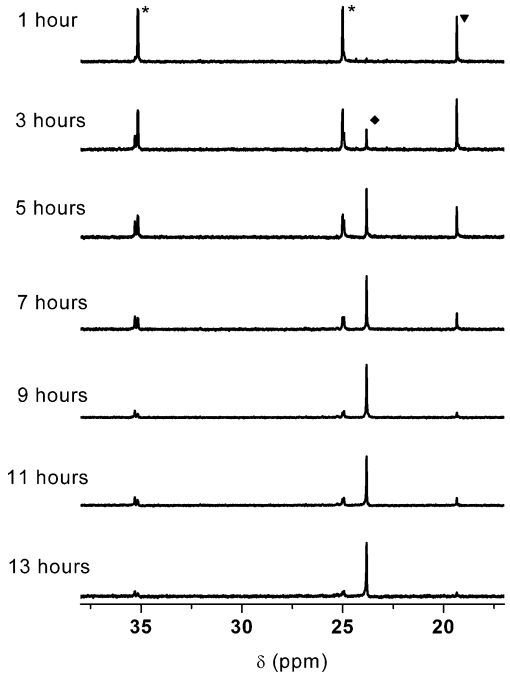

Figure 4. Time-dependent 500 MHz ^{31}P NMR spectra of a CD_3CN solution of *unsym*-3 at 60 °C. * Indicates signals for *unsym*-**3**; ▼ denotes intermediate isomer *meso*-3; ◆ represents signal for *sym*-**3**. Thus, the gradual disappearance of *unsym*-**3** accompanies the appearance of an intermediate at 19.7 ppm. Note also the transient formation of an unsymmetrical intermediate with chemical shifts close to those for *unsym*-**3**.

meso-**3** is the appearance of an unsymmetrical species, the ^{31}P NMR pattern of which is quite similar to that for *unsym*-**3**. The isomerization from *unsym*-**3** to *sym*-**3** could also be monitored by FT-IR spectroscopy in the ν_{CO} region, and through such studies we confirmed that addition of 10% Et_4NCN did not affect the rate of isomerization of *unsym*-**3** to *sym*-**3**.

C. $[Fe_2(S_2C_2H_4)(\mu\text{-}CO)(CN)_4(CO)_2]^{2-}$. Oxidative decarbonylation of $(Et_4N)_2$(**1**) in the presence of cyanide was found to be particularly efficient (Scheme 1). The synthesis was accomplished by the simultaneous addition of both $FcPF_6$ and Et_4NCN to a cold MeCN solution of $(Et_4N)_2$(**1**) under an atmosphere of CO. The red-colored product was separated from the cogenerated Et_4NPF_6 by precipitation of the latter from cold MeOH. The FT-IR spectrum of $[Fe_2(S_2C_2H_4)(\mu\text{-}CO)(CN)_4(CO)_2]^{2-}$ (**4**) consisted of the expected bands attributable to ν_{CN}, ν_{t-CO}, and $\nu_{\mu-CO}$. Dianion **4** was also cleanly formed by displacement of PPh_3 with CN^- from **2**. The corresponding reactions of Et_4NCN with *sym*- and *unsym*-**3** did not proceed cleanly, presumably indicative of the greater difficulty of displacing PMe_3 vs the weakly basic PPh_3.

The relative efficiency of the oxidation of $(Et_4N)_2$(**1**) in the presence of excess Et_4NCN prompted us to investigate the corresponding reaction using the propanedithiolate analogue. Indeed, $(Et_4N)_2[Fe_2(S_2C_3H_6)(\mu\text{-}CO)(CN)_4(CO)_2]$ is cleanly generated and exhibited the expected spectroscopic properties.

Oxidation of $(Et_4N)_2$(**1**) in the presence of only 1 equiv of Et_4NCN afforded an unstable red-colored species, assigned as $[Fe_2(S_2C_2H_4)(\mu\text{-}CO)(CN)_3(CO)_3]^-$ (**5**) (Scheme 1). In its FT-IR spectrum, the ν_{CO} bands are relatively high in energy (2073, 2048, 2022, 1927 cm^{-1}). The implied high electrophilicity is probably related to the compound's instability. For example, removal of solvent from solutions of **5** resulted in decomposition. Compound **5** was shown to cleanly convert to **4** upon treatment with 1 equiv of Et_4NCN (Scheme 1). Similarly, addition of PEt_3 to an MeCN solution of **5** afforded a single isomer of the adduct $[Fe_2(S_2C_2H_4)(\mu\text{-}CO)(CN)_3(CO)_3(PEt_3)_2]^-$ (**6**, Scheme 1). In contrast to its precursor, **6** was sufficiently stable to be characterized by IR, ESI-MS, and ^{31}P NMR spectroscopy.

Attempted Reduction of H_{ox}^{CO} Models to H_{red} Models. The electrochemical and chemical reduction of **2**, *sym*-**3**, and **4** were surveyed. Cyclic voltammetry of **2** in MeCN solution revealed a reversible reduction at −555 mV vs Ag/AgCl, while the related PMe_3 derivative *sym*-**3** requires a potential of −894 mV. The dianionic tetracyanide **4** irreversibly reduced at −985 mV. In all three cases, only one reduction process was observed. Treatment of **2** with 1 equiv of Cp_2Co gave ca. 50% yield of **1** together with unreacted starting material. Using 2 equiv of Cp_2Co, **2** cleanly gave **1**, as verified by IR spectroscopy (Scheme 1), indicative of a 2e$^-$ process.

Density Functional Theory Calculations. Twelve diastereomers are possible for $[Fe(CN)(PMe_3)(CO)]_2(\mu\text{-}CO)(S_2C_nH_{2n})$, corresponding to six isomers derivable from a C_s symmetric parent (**3.2**), while the other six isomers come from a C_2 symmetric parent (**3.1**). The DFT structures of the relevant isomers of **3** are shown in Figure 5, while corresponding relative energies, IR frequencies, and Fe−Fe and Fe−μ-CO distances are collected in Table 2. Assuming that an Fe−μ-CO bond breaks to enable turnstile rotation of the $Fe(CN)(CO)(PMe_3)$ vertex, the six isomers related to **3.1** are mutually interconvertable, as are the other isomers, but these two sets cannot interconvert by ordinary turnstile mechanisms.

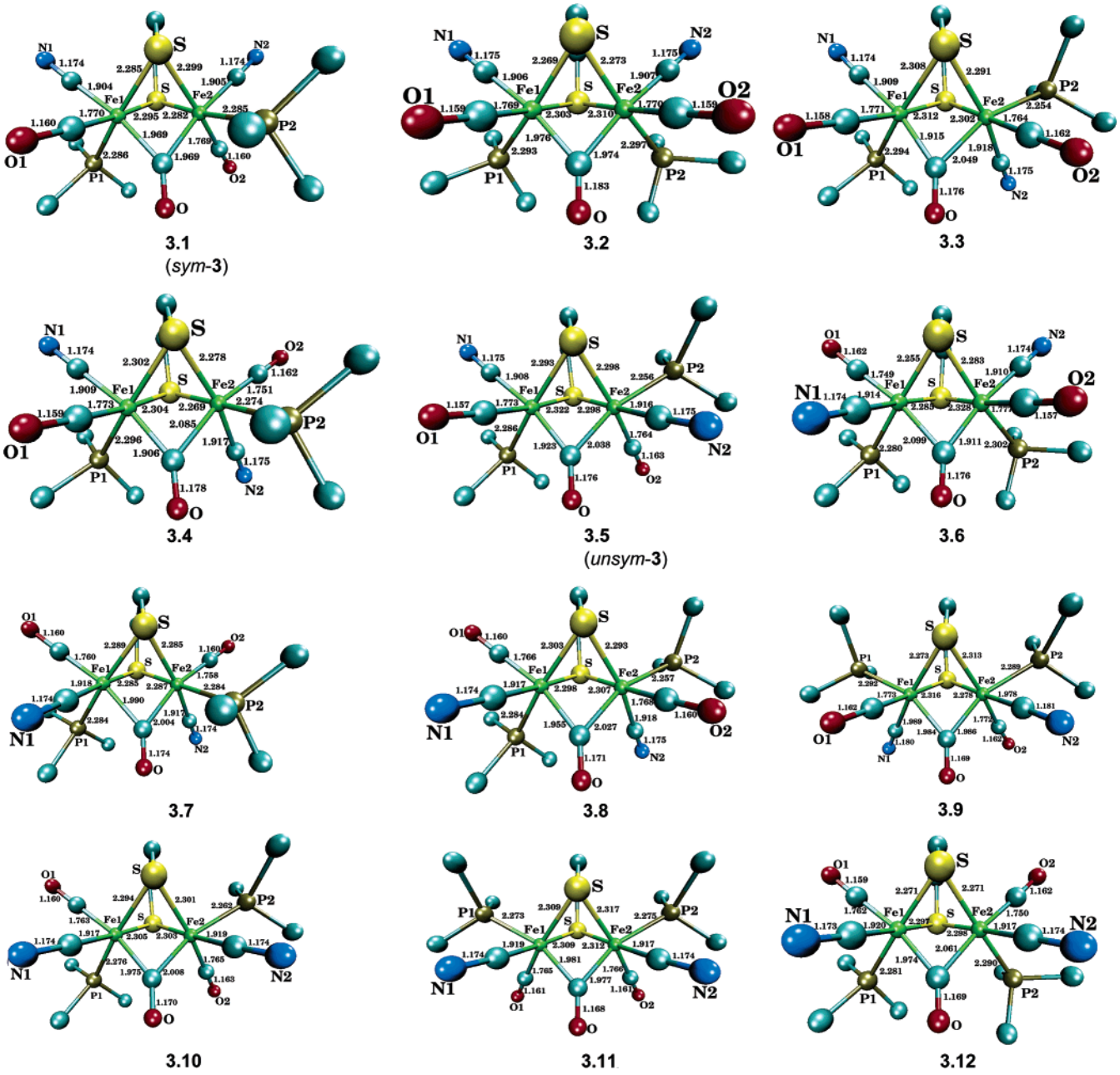

Figure 5. DFT-optimized structures of the twelve possible diastereomers for $Fe_2(S_2C_2H_4)(\mu\text{-CO})(CN)_2(PMe_3)_2(CO)_2$ (**3**).

The comparison of structures and energies revealed that isomers featuring CO and/or PMe_3 groups trans to the μ-CO ligand are less stable than isomers with CN^- trans to μ-CO. Furthermore, placing the PMe_3 ligand in the basal arrangement results in less distortion of the iron environment from octahedral geometry than isomers featuring one or two axial PMe_3 groups (not shown). Analysis of the isomers featuring CO and/or PMe_3 groups trans to the μ-CO suggested, however, that the origin of the destabilization was mainly electronic. Supporting this view, the Fe$-\mu$-CO distance is most strongly affected by the identity of the trans ligand. This effect can be partly attributed to the competition for π electrons by mutually trans π-acceptors. Consistent with these considerations, the less stable $[Fe_2(S_2C_2H_4)(\mu\text{-CO})(CN)_2(PMe_3)_2(CO)_2]$ isomers (**3.7**$-$**3.12**) are characterized by the presence of CO and/or PMe_3 ligands trans to μ-CO ligand.

The crystallographically characterized isomer of $Fe_2(S_2C_2H_4)(\mu\text{-CO})(CN)_2(PPh_3)_2(CO)_2$ is analogous to the computed complex **3.5**, which is shown to be only 5.7 kcal/mol less stable than **3.1** (Table 2). Notably, and in very good agreement with X-ray data, the μ-CO ligand is bridged in an asymmetric fashion, with the two Fe$-\mu$-CO bond distances differing by more than 0.1 Å (Figure 2, **3.5**). As discussed above, the peculiar geometry of **3.5** (and **3.3**, which is slightly more stable and differs only by the relative position of the basal CO and CN^- groups on Fe2) is due to the ligands trans to the μ-CO group. Cyanide trans to μ-CO leads to shortened Fe$-\mu$-CO bonds.

The effects of the nature of the ligands trans to the μ-CO ligand is reflected not only in a modulation of key geometry parameters but also in the corresponding IR spectra. IR spectra computed for **3.1** and **3.2** are similar (Table 2) and in reasonable agreement with the corresponding experimental data. In par-

Table 2. Summary of DFT Calculations for Isomers of $Fe_2(S_2C_2H_4)(\mu\text{-CO})(CN)_2(PMe_3)_2(CO)_2$

model	ΔE (referred to isomer **3.1**; kcal mol^{-1})	CN, CO frequencies (cm^{-1}) [experimentally observed]	Fe1–Fe2; Fe–μ-CO distances (Å) [experimentally observed]
3.1	0	1814; 1993; 2003; 2132; 2134	2.495; 1.969; 1.969
		[1839; 2003; 2020; 2115 (*sym*-**3**)]	
3.2	2.0	1830; 1996; 2012; 2128; 2129	2.509; 1.974; 1.976
3.3	3.9	1870; 1985; 2015; 2121; 2130	2.517; 1.915; 2.049
3.4	4.8	1856; 1987; 2007.56; 2126; 2133	2.519; 1.906; 2.085
3.5	5.7	1871; 1978; 2019; 2127; 2131	2.515; 1.923; 2.038
		[1904; 1993; 2039; 2104; 2119 (**2**)]	[2.55; 1.85; 2.15]
		[1884; 1992; 2032; 2107; 2117 (*unsym*-**3**)]	
3.6	9.5	1868; 1984; 2019; 2130; 2133	2.535; 2.099; 1.911
3.7	11.1	1874; 1992; 2001; 2131; 2131	2.516; 1.990; 2.004
3.8	12.7	1896; 1991; 2002; 2121; 2137	2.525; 1.955; 2.027
3.9	14.8	1916; 1992; 2004; 2128; 2129	2.489; 1.984; 1.986
3.10	15.4	1897; 1979; 1998; 2131; 2138	2.527; 1.975; 2.008
3.11	16.1	1913; 1983; 2002; 2130; 2131	2.530; 1.981; 1.977
3.12	20.3	1901; 1984; 2002; 2133; 2140	2.550; 1.974; 2.061

ticular, strong back-donation from both Fe centers to the μ-CO ligand results in a weakening of the CO bond, with consequent shift of CO stretching frequencies to lower values (1814 and 1830 cm^{-1} for **3.1** and **3.2**, respectively). The progressive exchange of CN^- ligands with PMe_3 or CO ligands, as observed going from **3.1** to **3.12**, results in a dramatic shift to higher values of the μ-CO IR frequency, confirming the extent to which ν_{CO} can be tuned.

Another stable isomer is **3.4**, where both the PMe_3 groups are basal, whereas a CO and a CN^- group have axial orientation. Isomer **3.4** differs from **3.3** only by the exchange of the PMe_3 and CO ligands coordinated to Fe2. As observed in **3.3** and **3.5**, the μ-CO group is coordinated in an unsymmetrical fashion in **3.4**. The computed IR frequencies for **3.4** (Table 2) quite closely resemble those computed for **3.3** and **3.5**, although agreement is *not* excellent for $\nu_{\mu-CO}$.

Conclusions

Oxidative Decarbonylation. The oxidative decarbonylation of diiron(I) dithiolates is shown to be a powerful method for generating previously unknown diferrous cyanides. This conversion is initiated by the oxidation of suitable diiron dithiolates that are more reducing than ferrocene (~400 mV vs SCE).[31] Upon oxidation, the diiron dithiolate requires additional donor ligands to stabilize the corresponding Fe^{II} oxidation states, as illustrated by the successful preparation of tricyanide **5** vs the decomposition of $(Et_4N)_2$**1** upon oxidation without any additional CN^- present. Even this tricyano-tetracarbonyl species is labile and highly reactive toward nucleophiles such as CN^- and PEt_3, which readily afford isolable adducts. This set of experiments may guide future applications of the oxidative decarbonylation method whereby nucleophiles can be installed *subsequent* to the oxidation step, thus minimizing potential incompatibilities between electrophilic oxidants and nucleophilic trapping agents.

The new dithiolates resemble the H_{ox}, H_{ox}^{CO}, and H_{ox}^{air} states of Fe-only hydrogenases by virtue of the presence of the $Fe_2(SR)_2(\mu\text{-CO})(CN)_2(CO)_2L_2$ coordination sphere. The influence of the chelating dithiolate is indicated by the contrasting structures of $[Fe_2(S_2C_2H_4)(\mu\text{-CO})(CN)_4(CO)_2]^{2-}$ (**4**) vs $[Fe_2(SEt)_2(CN)_4(CO)_4]^{2-}$.[26] The chelating dithiolate destabilizes the edge-shared bioctahedral structures.

Isomerism. A challenge to modeling the active site of the Fe-only hydrogenases is the stereochemistry of the terminal ligands on the diiron core. In the case of $[FeLL'L'']_2(\mu\text{-CO})(S_2C_nH_{2n})$, 12 diastereoisomers are possible. The dinuclear active site of H_{ox}^{CO} has nine diastereomeric possibilities reflecting its simplified ligand set $[Fe(CO)(CN)L][Fe(CO)_2(CN)](\mu\text{-CO})(S_2C_nH_{2n})$ (where L is the thiolate of the 4Fe-4S cluster). Despite the potential for isomeric complexity, only one isomer is observed spectroscopically in the protein for the oxidized states H_{ox}, H_{ox}^{CO}, and H_{ox}^{air}.[8,9] The situation for H_{red} is less clear, as reflected by the complexity of its IR spectrum in the ν_{CO} region;[4] i.e., it is possible that in H_{red} isomers coexist.

In this paper we demonstrated that if isomerism existed in the oxidized states of the protein, such isomers would be readily distinguished using IR spectroscopy. Intriguing questions persist as to the reason that the CN^- ligands in the H-cluster are basal vs the diaxial geometry that is energetically preferred by the model systems examined in this paper. We can envision several factors that could stabilize the dibasal structure. In H_{ox} and H_{red}, strong σ donors, OH^- and H^-, respectively, would also stabilize the trans μ-CO.[32] Crystallographic analyses reveal numerous hydrogen-bonding contacts between the protein backbone and the two cyanide ligands (Figure 6). These interactions could dictate the stereochemistry of the cyanide ligands as well as weaken their σ-donor properties.

Four isomers of $Fe_2(S_2C_2H_4)(\mu\text{-CO})(CN)_2(PR_3)_2(CO)_2$ were observed in this work; two were isolated. In contrast to the relatively slow isomerization for these diferrous species, isomerism is a low energy process for the usual $[Fe^IL(CO)_2]_2(\mu\text{-}S_2C_nH_{2n})$ species reflecting the facility of turnstile rotation at the formally five-coordinate $Fe(\mu\text{-SR})_2L_3$ centers.[34] For the confacial bioctahedral diferrous species, we suggest that isomerization begins with rupture of an Fe−μ-CO bond followed by turnstile rotation at the resulting $Fe(CO)(CN)(PMe_3)$ center. The asymmetric Fe−μ-CO−Fe bonding mode is consistent with this mechanism, the longer bond being to the Fe center that must undergo the isomerization according to the pathway proposed in eq 2. Also consistent with an intramolecular mechanism is

(31) Connelly, N. G.; Geiger, W. E. *Chem. Rev.* **1996**, *96*, 877−922.

(32) Bruschi, M.; Fantucci, P.; De Gioia, L. *Inorg. Chem.* **2004**, *43*, 4733.

(33) Peters, J. W.; Lanzilotta, W. N.; Lemon, B. J.; Seefeldt, L. C. *Science* **1998**, *282*, 1853−1858.

(34) Lyon, E. J.; Georgakaki, I. P.; Reibenspies, J. H.; Darensbourg, M. Y. *J. Am. Chem. Soc.* **2001**, *123*, 3268−3278.

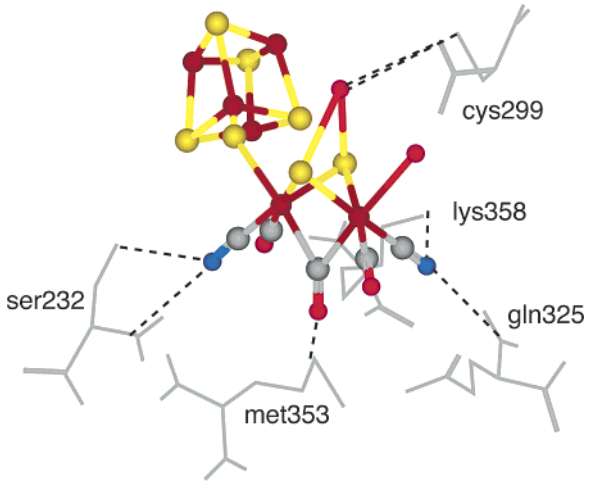

Figure 6. H-cluster active site from *C. pasteuranium* hydrogenase I showing hydrogen bonding interactions involving the CN^- ligands as well as the met- - -OC(μ) and dithiolate- - -HScys interactions.[33]

the observation that Et_4NCN does not affect the rate of interconversion.

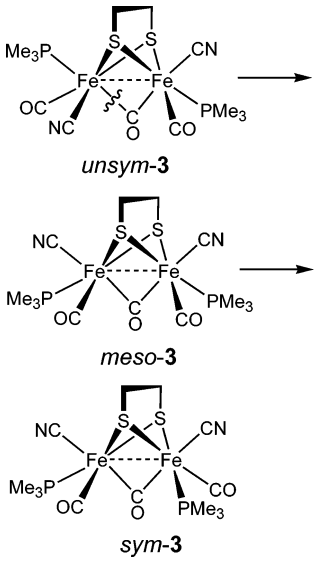

(2)

Considerations that guide this mechanism are that intermediates with two COs, $(PMe_3)(CO)$, or two PMe_3 ligands in axial positions are high-energy species, as indicated by the DFT calculations. The subsequent conversion of proposed *meso*-isomer to the *d,l*-diastereomer (**3.2** to **3.1**) requires interchange of terminal ligands. This conversion is accompanied by the formation of an apparent intermediate with ^{31}P NMR chemical shifts such as those for *unsym*-**3**. We suggest that this species has structure **3.3**. Further analysis of the associated mechanistic aspects will be pursued with other substituted derivatives in a future paper. The described diferrous compounds are stereochemically related to the species obtained by protonation of diiron(I) precursors, i.e., $[Fe_2(SR)_2(\mu\text{-H})(CO)_4L_2]^z$. Isomerization in such bioctahedral $(\mu\text{-SR})_2(\mu\text{-H})$ species is sufficiently slow that individual isomers can be detected by NMR spectroscopy.[35]

Comments on $\nu_{\mu-CO}$. The new complexes demonstrate that $\nu_{\mu-CO}$ is highly dependent on coligands and stereochemistry (Figure 7). A striking demonstration of the sensitivity of the $\nu_{\mu-CO}$ band is that *sym*-**3** features a $\nu_{\mu-CO}$ peak at 1839 cm^{-1}, which is 45 cm^{-1} lower than that for *unsym*-**3** (1884 cm^{-1}); this difference indicates the dominant influence of the trans ligands. Further demonstration of the sensitivity of $\nu_{\mu-CO}$ can be seen upon methylation of the CN^- ligands in compound **4**, which leads to a shift in ν_{CO} from 1876 to 1969 cm^{-1} for $[Fe_2(S_2C_2H_4)(\mu\text{-CO})(CN)_4(CO)_2]^{2-}$ and $[Fe_2(S_2C_2H_4)(\mu\text{-CO})(CNMe)_4(CO)_2]^{2+}$.[22] An overview of the broad range of the μ-CO IR bands as found in our $Fe^{II}Fe^{II}$ model compounds is shown in Figure 7.

One benchmark for comparing synthetic models to $H_{ox}{}^{air}$ is the position of the $\nu_{\mu-CO}$ band in the IR spectrum. This absorption occurs at 1847 cm^{-1} in the DdH enzyme.[36] The fact that the enzyme has such a low frequency suggests that the ligands trans to μ-CO are powerful donors, which is consistent with the presence of hydroxide.[37] Diiron dithiolates containing such hard anionic ligands are not known.

Experimental Section

General Procedures. Methods and materials were recently described.[22]

$Fe_2(S_2C_2H_4)(\mu\text{-CO})(CN)_2(PPh_3)_2(CO)_2$ (2). An orange solution of 0.10 g (0.16 mmol) of $(Et_4N)_2[Fe_2(S_2C_2H_4)(CN)_2(CO)_4]$ and 0.21 g (0.80 mmol) of PPh_3 in 20 mL of MeCN and 5 mL of toluene was saturated with CO and cooled to −40 °C. The reaction mixture was treated with a solution of 0.105 g (0.32 mmol) of $[Cp_2Fe]PF_6$ in 5 mL of MeCN. After stirring for 2 min, the solution was concentrated in vacuo to ~5 mL. Addition of 50 mL of Et_2O precipitated a brown solid leaving a yellow solution of Cp_2Fe. The brown solid was extracted into toluene, and the extract was filtered through Celite to remove Et_4NPF_6. The resulting red-brown solution was concentrated in vacuo to ~5 mL. Addition of hexanes precipitated the product. This solid was taken up in 5 mL of CH_2Cl_2, and this extract was passed through a 32 × 3.5 cm column of silica gel, eluting with CH_2Cl_2, MeCN, and MeOH. The third band (and largest band) was concentrated to 5 mL and diluted with 50 mL of hexane to precipitate a brown powder. Single crystals, suitable for X-ray analysis, were grown by slow evaporation of a CH_2Cl_2 solution. Yield: 0.014 g (10%). Anal. Calcd for $C_{43}H_{34}Fe_2N_2O_3P_2S_2$: C, 59.74; H, 3.96; N, 3.24. Found: C, 60.26; H, 4.79; N, 3.03. ^{31}P NMR (202 MHz, CD_3CN): δ 46.3 (s), 71.2 (s). FT-IR (MeCN, cm^{-1}): ν 2119 (m), 2104 (m), 2039 (s), 1993 (s), 1904 (w) cm^{-1}. ESI-MS (*m*/*z*): 864 $\{Fe_2(S_2C_2H_4)(\mu\text{-CO})(CN)_2(PPh_3)_2(CO)_2\}$, 1729 $\{Fe_2(S_2C_2H_4)(\mu\text{-CO})(CN)_2(PPh_3)_2(CO)_2\}_2$. FAB-MS (*m*/*z*): 864 $\{Fe_2(S_2C_2H_4)(\mu\text{-CO})(CN)_2(PPh_3)_2(CO)_2\}$.

$Fe_2(S_2C_2H_4)(\mu\text{-CO})(CN)_2(PMe_3)_2(CO)_2$ (*unsym*-3). An orange solution of 0.10 g (0.16 mmol) of $(Et_4N)_2[Fe_2(S_2C_2H_4)(CN)_2(CO)_4]$ in 20 mL of MeCN was saturated with CO and cooled to −40 °C. The reaction mixture was treated with a solution of 0.105 g (0.32 mmol) of $[Cp_2Fe]PF_6$ in 5 mL of MeCN and 0.08 mL (0.8 mmol) of PMe_3 in 5 mL of MeCN *simultaneously* followed by stirring for 2 min. The volume of the resulting brown solution was reduced in vacuo to approximately 5 mL. Addition of 50 mL of Et_2O precipitated a brown solid leaving a yellow solution of Cp_2Fe. An extract of this solid in 5 mL of CH_2Cl_2 was purified by chromatography on silica gel, eluting with CH_2Cl_2. The third band (and largest band) was concentrated in vacuo to 5 mL, and the concentrated solution was diluted with 50 mL of hexane to precipitate *unsym*-**3** as a brown powder. Yield: 0.012 g (15%). Anal. Calcd for $C_{13}H_{22}Fe_2N_2O_3P_2S_2$: C, 31.73; H, 4.51; N, 5.96. Found: C, 31.79; H, 4.58; N, 5.53. ^1H NMR (500 MHz,

(35) Zhao, X.; Hsiao, Y.-M.; Lai, C.-H.; Reibenspies, J. H.; Darensbourg, M. Y. *Inorg. Chem.* **2002**, 699−708.
(36) Nicolet, Y.; de Lacey, A. L.; Vernède, X.; Fernandez, V. M.; Hatchikian, E. C.; Fontecilla-Camps, J. C. *J. Am. Chem. Soc.* **2001**, *123*, 1596−1601.
(37) Bruschi, M.; Fantucci, P.; De Gioia, L. *Inorg. Chem.* **2003**, *42*, 4773−4781.

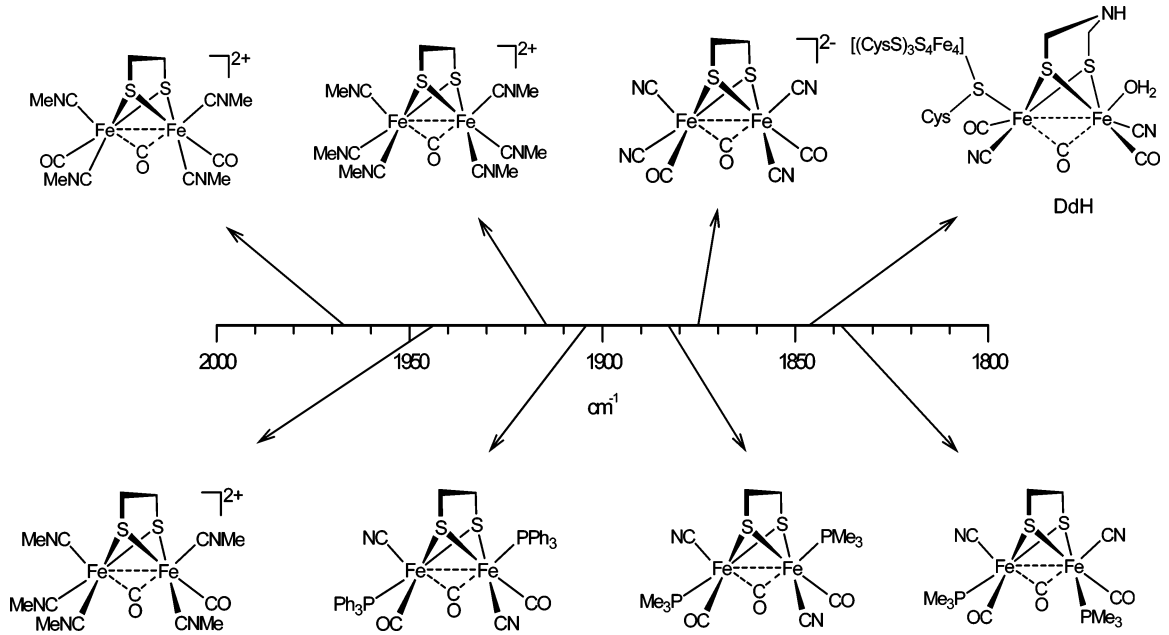

Figure 7. Schematic overview of "tuning" $\nu_{\mu-CO}$ in synthetic $Fe^{II}Fe^{II}$ complexes.

CD_3CN): δ 1.60 (d, 9H, PMe_3, J_{P-P} 11 Hz), 1.79 (d, 9H, PMe_3, J_{P-P} 11 Hz), 2.60 (m, 1H, edt), 2.92 (m, 1H, edt), 3.04 (m, 1H, edt), 3.18 (m, 1H, edt). ^{31}P NMR (202 MHz, CD_3CN): δ 25.0 (d, J_{P-P} 6 Hz), 35.1 (d, J_{P-P} 6 Hz). FT-IR (MeCN, cm^{-1}): ν 2117 (m), 2107 (m), 2032 (s), 1992 (s), 1884 (w). FAB-MS (*m*/*z*): 492.0 $\{Fe_2(S_2C_2H_4)$-$(\mu$-CO)$(CN)_2(PMe_3)_2(CO)_2\}$.

$Fe_2(S_2C_2H_4)(\mu$-CO)$(CN)_2(PMe_3)_2(CO)_2$ (*sym*-3). A solution of 0.15 g of (0.32 mmol) $Fe_2(S_2C_2H_4)(CO)_4(PMe_3)_2$ in 30 mL of MeCN was cooled to −40 °C under a stream of CO and then treated with a solution of 0.24 g (0.73 mmol) of $[Cp_2Fe]PF_6$ in 10 mL of MeCN. After 20 min, a solution of 0.13 g (0.83 mmol) of Et_4NCN in 10 mL of MeCN was added. The reaction mixture was stirred for an additional 20 min at −40 °C before being allowed to warm to room temperature. Solvent was removed in vacuo to leave a crude brown solid. The product was extracted twice with 30 mL portions of toluene; the extract was evaporated to dryness, and the brown residue was washed with 25 mL of hexane. Yield: 0.040 g (25%). ^{1}H NMR (500 MHz, CD_3CN): δ 1.57 (d, 18H, PMe_3, J_{P-H} = 10.5 Hz), 3.08 (m, 4H, SCH_2CH_2S). ^{31}P NMR (202 MHz, CD_3CN): δ 23.8 (s). FT-IR (toluene, cm^{-1}): ν = 2115 (w), 2020 (sh, m), 2003 (s), 1839 (w). Anal. Calcd for $C_{13}H_{22}Fe_2N_2O_3P_2S_2$: C, 31.73; H, 4.51; N, 5.96. Found: C, 32.01; H, 4.56; N, 5.83. FAB-MS (*m*/*z*) 491.9 (100% [M]).

$(Et_4N)_2[Fe_2(S_2C_2H_4)(\mu$-CO)$(CN)_4(CO)_2]$ (4). An orange solution of 0.10 g (0.16 mmol) of **1** in 20 mL of MeCN was saturated with CO and cooled to −40 °C. The reaction solution was treated *simultaneously* with a solution of 0.105 g (0.32 mmol) of $[Cp_2Fe]PF_6$ in 5 mL of MeCN and 0.050 g (0.32 mmol) of Et_4NCN in 5 mL of MeCN followed by stirring for 2 min. The resulting red-brown solution was concentrated in vacuo to ca. 5 mL and then diluted with 50 mL of Et_2O to precipitate a brown solid leaving a yellow solution of Cp_2Fe. The solid was extracted into MeOH. Cooling this extract to ca. −90 °C precipitated Et_4NPF_6, which was removed by filtration. After rewarming to room temperature, the solution was concentrated in volume in vacuo and diluted with 50 mL of Et_2O to precipitate the brown powder. Yield: 0.074 g (70%). Anal. Calcd for $C_{25}H_{44}Fe_2N_4O_3S_2$ H_2O: C, 44.78; H, 6.92; N, 12.53. Found: C, 44.31; H, 6.90; N, 12.31. FT-IR (MeCN, cm^{-1}): 2109 (w), 2012 (s), 1990 (s), 1876 (w). ESI-MS (*m*/*z*): 522, $\{(Et_4N)[Fe_2(S_2C_2H_4)(\mu$-CO)$(CN)_4(CO)_2]\}^-$; 1174, $\{(Et_4N)_3[Fe_2(S_2C_2H_4)$-$(\mu$-CO)$(CN)_4(CO)_2]_2\}^-$.

$(Et_4N)[Fe_2(S_2C_2H_4)(\mu$-CO)$(CN)_3(CO)_3]$ (5). An orange solution of 0.10 g (0.16 mmol) of **1** in 20 mL of MeCN was saturated with CO and cooled to −40 °C. The reaction solution was treated with a solution of 0.105 g (0.32 mmol) of $[Cp_2Fe]PF_6$ in 5 mL of MeCN and 0.025 g (0.16 mmol) of Et_4NCN in 5 mL of MeCN *simultaneously*, followed by stirring for 2 min. Hexane was added to remove ferrocene in a biphasic extraction, leaving a red MeCN solution containing the product and Et_4NPF_6. FT-IR (MeCN, cm^{-1}): 2121 (w), 2073 (s), 2048 (s), 2022 (m), 1928 (w). ESI-MS (*m*/*z*): 394, $\{[Fe_2(S_2C_2H_4)(\mu$-CO)$(CN)_3$-$(CO)_3]\}^-$; 669, $\{(Et_4NPF_6)[Fe_2(S_2C_2H_4)(\mu$-CO)$(CN)_3(CO)_3]\}^-$.

To the solution of **5** in MeCN was added 0.025 g (0.16 mmol) of Et_4NCN under a CO atmosphere at −40 °C. After warming the reaction to room temperature, solvent was concentrated in vacuo to 5 mL. Addition of 50 mL of Et_2O precipitated a brown powder spectroscopically identified as **4**.

$(Et_4N)[Fe_2(S_2C_2H_4)(\mu$-CO)$(CN)_3(CO)_2(PEt_3)]$. To the solution of **5** in MeCN, prepared as described above, was added 0.2 mL (1.6 mmol) of PEt_3 under a CO atmosphere at −40 °C. Upon warming the solution to room temperature, the solvent was concentrated in vacuo to 5 mL, and the addition of 50 mL of Et_2O precipitated a brown powder spectroscopically identified as $(Et_4N)[Fe_2(S_2C_2H_4)(\mu$-CO)$(CN)_3(PEt_3)(CO)_2]$. ^{31}P NMR (202 MHz, CD_3CN): δ 65.7 (s). FT-IR (MeCN, cm^{-1}): 2120 (w), 2116 (w), 2103 (w), 2025 (s), 1978 (s), 1898 (w). ESI-MS (*m*/*z*): 484$\{[Fe_2(S_2C_2H_4)(\mu$-CO)$(CN)_3(CO)_2(PEt_3)]\}^-$, 759 $\{(Et_4N)(PF_6)$-$[Fe_2(S_2C_2H_4)(\mu$-CO)$(CN)_3(CO)_2(PEt_3)]\}^-$.

Computational Methods. Calculations have been carried out using the Turbomole suite of programs[38] in connection with the resolution of the identity technique.[39,40] Structure optimizations have been carried out within the density functional theory formalism using the BP86 functional[41,42] and an all-electron valence triple-ζ basis set with polarization functions on all atoms (TZVP).[43] The adopted level of theory was already shown to be well suited to investigate models of the Fe-hydrogenase active site.[44] Stationary points on the energy

(38) Ahlrichs, R.; Baer, M.; Haeser, M.; Horn, H.; Koelmel, C. *Chem. Phys. Lett.* **1989**, *162*, 165−169.
(39) Eichkorn, K.; Treutler, O.; Oehm, H.; Haeser, M.; Ahlrichs, R. *Chem. Phys. Lett.* **1995**, *240*, 283−290.
(40) Eichkorn, K.; Weigend, F.; Treutler, O.; Ahlrichs, R. *Theor. Chem. Acc.* **1997**, *97*, 119−124.
(41) Becke, A. D. *Phys. Rev.* **1988**, *A38*, 3098−3100.
(42) Perdew, J. P. *Phys. Rev.* **1986**, *B33*, 8822−8824.
(43) Schaefer, A.; Huber, C.; Ahlrichs, R. *J. Chem. Phys.* **1994**, *100*, 5829−5835.
(44) Zampella, G.; Bruschi, M.; Fantucci, P.; Razavet, M.; Pickett, C. J.; De Gioia, L. *Chem.—Eur. J.* **2005**, *11*, 509−520.

hypersurface have been located by means of energy gradient techniques. Full vibrational analysis has been carried out to further characterize each stationary point.

Acknowledgment. This research was supported by NIH. We thank Maurizio Bruschi for helpful advice.

Supporting Information Available: X-ray crystallographic file (in CIF format) for complex *unsym*-**3**. This material is available free of charge via the Internet at http://pubs.acs.org.

JA051584D